Synthesis of magnetically separable ordered mesoporous carbons using furfuryl alcohol and cobalt nitrate in a silica template†

In-Soo Park,‡ Minkee Choi, Tae-Wan Kim and Ryong Ryoo*

Received 22nd March 2006, Accepted 29th June 2006
First published as an Advance Article on the web 18th July 2006
DOI: 10.1039/b604228g

Synthesis of ordered mesoporous carbons containing Co, Ni, and Fe nanoparticles within the mesostructure was performed through carbonization of poly(furfuryl alcohol) in the presence of metal nitrate inside SBA-15 mesoporous silica templates. The use of the transition metal nitrates, instead of Al catalyst, led also to the formation of highly ordered mesoporous carbons having the same structure as CMK-3. The 2-dimensionally hexagonal *p6mm* structure was constructed from a regular array of uniform nanopores (typically 4–5 nm in diameter) and carbon frameworks (typically 4 nm in thickness). The state of the materials during the carbonization process was characterized by X-ray diffraction, nitrogen physisorption, transmission electron microscopy, and X-ray absorption fine structure spectroscopy of the metal elements. The results showed that metal nanoparticles, 25–40 nm in diameter, were embedded inside the mesoporous carbon networks. The nanoparticles were formed due to spontaneous reduction of the metal elements during carbonization, following the initial action as a catalyst for the polymerization of furfuryl alcohol. The magnetic hysteresis loop for the cobalt-containing carbon showed soft ferromagnetic behaviour at room temperature. In particular, the cobalt nanoparticles could be protected against acidic erosion by repeating impregnation and polymerization of furfuryl alcohol once more before its carbonization treatment. The process is proposed as a method for preparation of magnetically separable mesoporous carbons, for application as an adsorbent or catalyst support.

1. Introduction

In recent years, synthesis of ordered mesoporous carbons (OMC) using silica templates has attracted much attention due to the structural ordering of pores, uniform pore diameters, high specific surface area, high stability, and facile functionalization of such mesostructured carbons.[1–4] Mesoporous carbons are available with various structures such as cubic *Ia3d*, *Fm3m*, *Im3m*, and 2-dimensionally (2-D) hexagonal *p6mm*. The pore diameter and pore-wall thickness are variable according to the structure of the silica template and other details of the synthesis conditions.[5] Various organic compounds including sucrose,[1,2,5] furfuryl alcohol,[3] ethylene,[6] acenaphthene,[7] and a phenol–formaldehyde[8] mixture are suitable as the carbon sources. The carbon precursors are converted to a rigid, 3-D carbon framework in the mesoporous silica templates, following a high-temperature carbonization process. The structural order of the carbon framework is self-retained after the silica template is removed with NaOH or HF solution.

National Creative Research Initiative Center for Functional Nanomaterials and Department of Chemistry (School of Molecular Science-BK21), Korea Advanced Institute of Science and Technology, Daejeon, 305-701, Republic of Korea. E-mail: rryoo@kaist.ac.kr; Fax: +82 42 869 8130; Tel: +82 42 869 2830

† Electronic supplementary information (ESI) available: design of XAFS cell; XRD patterns for NiCMK carbons and FeCMK carbons. See DOI: 10.1039/b604228g

‡ Current address: Department of Chemical & Biological Engineering, Korea University, Anam-dong, Seongbuk-ku, Seoul, 136-713, Republic of Korea.

Furfuryl alcohol is most widely used as a carbon source for OMC materials.[3,9,10] The advantages of furfuryl alcohol are its facile impregnation into the template pores in the liquid phase or through vapor adsorption, polymerization into cross-linked polymers, and carbonization into rigid frameworks. The carbon framework has a tube-like (hollow) or rod-like structure, depending on the details of the synthesis conditions.[3,11] The polymerization can be carried out by the addition of an organic acid into furfuryl alcohol,[11,12] or the generation of solid acid sites through impregnation of Al onto the silica pore walls prior to loading of the carbon source.[3] Catalytic sites may also be generated by impregnation of transition metal compounds.[13,14] Polymerization using Co, Ni, and Fe compounds is particularly attractive because these metal elements may be incorporated in the final OMC products, thus affording the possibility to prepare OMC materials containing magnetisable metal nanoparticles. OMC materials containing such magnetic nanoparticles may find suitable applications for the development of heterogeneous catalysts and adsorbents that can be separated by a magnetic field after use in the liquid phase.[15–17] Similarly, there has been strong interest in recent years in the preparation of magnetically separable mesoporous silicas such as MCM-41, MCM-48, and SBA-15 containing iron oxide or cobalt nanoparticles.[18]

The present work was undertaken to prepare magnetically separable OMC materials using furfuryl alcohol, Co, Ni, and Fe nitrates. SBA-15 silica[19] was selected as a template for the OMC materials. SBA-15 silica is a mesoporous material with a 2-D hexagonal structure, in which 1-D mesoporous channels are randomly interconnected through complementary pores.[20]

The synthesis results showed that metal nanoparticles, 25–40 nm in diameter, were embedded inside the porous carbon particles. The OMC products containing the nanoparticles were attracted by an external magnetic field, suggesting strong potential for applications in magnetic separation. Furthermore, in some cases, the OMC products exhibited magnetic attraction even after washing with strong acid. This interesting result motivated us to investigate the detailed effects of the OMC synthesis procedure. The investigation was performed by materials characterization with X-ray diffraction (XRD), nitrogen adsorption, transmission electron microscopy (TEM), and X-ray absorption fine structure spectroscopy (XAFS).

2. Experimental

2.1 Materials

Synthesis of mesoporous silica template. The SBA-15 silica was synthesized following the procedure reported by Choi *et al.*[20] In a typical synthesis batch, 69.1 g of the structure-directing triblock copolymer, $EO_{20}PO_{70}EO_{20}$ (EO = ethylene oxide, PO = propylene oxide, $M_n \sim 5800$, Aldrich), was dissolved in 522 g of 0.3 M HCl solution (35 wt%, Junsei) at 35 °C. 857 g of 5% sodium silicate (DC Chemical, 25 wt% SiO_2 in aqueous solution, Si/Na = 1.5) was added into the solution with vigorous stirring at 35 °C. Stirring was continued for 24 h at the same temperature, and the mixture was then heated in an autoclave at 150 °C for 24 h under static condition. The SBA-15 silica product was filtered after the reaction mixture was cooled to below 100 °C. The product was washed with distilled water and dried at 70 °C. The polymeric structure-directing agent was removed by extraction with an ethanol–HCl mixture and calcination for 2 h at 550 °C in air.

Synthesis of Co-containing OMC. Calcined SBA-15 silica was impregnated with an acetone solution containing metal nitrate. In a typical batch for 2 wt% Co loading on silica, 0.198 g of $Co(NO_3)_2 \cdot 6H_2O$ (97%, Junsei, vacuum dried at room temperature before use) was dissolved in 50 mL of acetone. This solution was agitated with 2.0 g of calcined SBA-15. Acetone was removed at 40 °C using a rotary evaporator. The resultant silica was further dried in an oven at 100 °C. The sample, which is designated as Co(2)SBA-15, was well mixed with 1.74 mL of furfuryl alcohol (98%, Daejung) at room temperature. This mixture was transferred into a fused quartz reactor, which was equipped with a porous plug or capillary cap to prevent the entry of air from outside while releasing gaseous by-products. The reactor was maintained at 35 °C for 1 h, in order to allow diffusion of furfuryl alcohol into the mesopores. Polymerization of the furfuryl alcohol was carried out by heating the sample to 105 °C over 1 h and subsequently maintaining it at the same temperature for 1 h. Carbonization was then carried out by further heating to 700 or 900 °C at a heating rate of 200 °C h^{-1}, and maintaining it at the maximum temperature for 2 h. The heating furnace was purged with an N_2 flow during the polymerization and carbonization process until the sample was cooled to room temperature after carbonization. After being cooled to room temperature, the product was opened in air and washed twice with sodium hydroxide solution (NaOH–ethanol–H_2O = 1 : 22 : 44 in mol ratio) to dissolve the silica template completely. The carbon product containing Co nanoparticles was filtered and dried in air at 100 °C. The carbon is designated as Co(2)CMK-700 or Co(2)CMK-900, according to the 2 wt% Co on SiO_2 used for the carbon preparation, and the carbonization temperature (700 or 900 °C). All Co-containing OMC samples were synthesized as described here, except those mentioned as *protected against acid leaching* in section 3.4.

Synthesis of self-protected Co-containing OMC. The synthesis procedure for the CoCMK samples mentioned as protected against acid leaching in section 3.4 is as follows: $Co(NO_3)_2 \cdot 6H_2O$ corresponding to 5 wt% Co was supported on SBA-15 as described above. 1.0 g of the CoSBA-15 sample was infiltrated with 0.757 mL of furfuryl alcohol at room temperature. The resultant sample was maintained for 1 h at 35 °C, 1 h at 105 °C, and then 2 h at 350 °C. After being cooled to room temperature, the sample was added to 0.534 mL furfuryl alcohol, and maintained at 35 °C, and heated at 105 °C again. The sample was subsequently heated to 900 °C under nitrogen atmosphere. The carbon product was collected by filtration after washing with NaOH.

2.2 Characterization

Powder XRD patterns were recorded with a Rigaku Multiplex diffractometer operating with Cu Kα radiation at 1.5 kW. For measurement with $2\theta \leqslant 3°$, the step width and acquisition time were 0.01° and 1.0 s, respectively; 0.02° and 0.5 s were employed for wider angles. Average particle size of metals or metal oxides were estimated by analysis of the most intense diffraction peak of the corresponding phase using the Scherrer equation[21] (JADE 5.0 software, Materials Data Inc.). For transmission electron microscopy (TEM), powder samples were dispersed in ethanol with sonication. Porous carbon grids were dipped into the suspension, and the dried grids were used. TEM images were obtained with a Philips F20 Tecnai instrument operating at 160 kV. Magnetic properties were measured at 17 °C with a conventional Vibrating Sample Magnetometer (VSM), using a Riken Denshi VT 800 instrument.

Nitrogen adsorption–desorption isotherms were obtained with a Quantachrome Autosorp-1MP instrument at −196 °C. Samples were outgassed for 10 h under vacuum at 300 °C before measurement. The specific surface area was calculated using the BET equation, using data in the P/P_0 region between 0.05 and 0.15. The BJH (Barret–Joyner–Halenda) method was applied to analyze the mesopore size distributions using the adsorption branch. Total pore volume was estimated from the amount of nitrogen adsorbed at a relative pressure of about 0.95. The sums of the primary mesopore and the micropore volumes were estimated from the α_s plot method in the range 1.7–2.2. The reference isotherm used for the α_s plot was adopted from the report by Kruk *et al.*[22]

For the X-ray absorption fine structures (XAFS) investigation, the Co(5)SBA-15 sample was pressed into 10 mm diameter pellets. Each pellet was impregnated with furfuryl alcohol and treated to a desired step for OMC synthesis, using

a specially designed reactor (shown in Fig. S1 of ESI†). After the reactor was cooled to room temperature, it was filled with N_2 gas. The XAFS cell part containing the sample pellet under N_2 was sealed by a flame. XAFS measurements were performed at the Co K-edge on BL7C1 at Pohang Light Source, with a ring current of 120–170 mA at 2.5 GeV. Si(311) monochromator crystals were used with detuning for the elimination of high-order harmonics. Data were collected in transmission mode using two N_2-filled ionization chambers. Energy calibration was carried out by assignment of the pre-edge inflection point to 7709 eV, using Co foil and an additional ionization chamber, where the chamber was placed following the second ionization chamber. The X-ray absorption near edge structures (XANES) were compared after pre-edge background removal and normalization of the absorption intensity. The extended X-ray absorption fine structures (EXAFS) were analyzed following the standard procedure using the IFEFFIT shell package.[23,24]

3. Results and discussion

3.1 OMC synthesis with furfuryl alcohol in CoSBA-15 template

Three OMC samples were synthesized using 2, 5 and 10% Co loadings on the same SBA-15 silica, and using the carbonization temperature of 700 °C. These carbons are designated as Co(2)CMK-700, Co(5)CMK-700 and Co(10)CMK-700, respectively. In Fig. 1, the XRD patterns of the OMC products are compared with that of original SBA-15 silica template. All the OMC materials in Fig. 1 show four distinct XRD lines which can be indexed according to the 2-D hexagonal structure. Note that both the CMK-3 and CMK-5 samples were synthesized using the aluminosilicate form of SBA-15 (AlSBA-15).[2,3] Despite the same 2D hexagonal *p6mm* structural symmetry, the framework structures show a significant difference between CMK-3 and CMK-5. CMK-3 is a faithful replica of SBA-15 silica, formed by replicating the mesoporous silica channels to rod-like carbon frameworks. In comparison, CMK-5 carbon is formed with tube-like, hollow carbon frameworks. Because of the structural difference, CMK-5 carbon shows a much lower (10)/(11) intensity ratio than CMK-3. The structural relation to the diffraction intensity was analyzed in a recent study using a continuous density functional technique.[25,26] According to the structural analysis by the (10)/(11) ratio, the Co(*m*)CMK-700 carbon samples correspond to an intermediate structure between the rod-type CMK-3 and the tube-type CMK-5 carbons. The detailed framework structure seem to be closer to tube-like in Co(2)CMK-700 than Co(10)CMK-700.

Fig. 2 shows N_2 adsorption–desorption isotherms of the Co(*m*)CMK-700 materials, and the pore size distribution (PSD) curves obtained from the adsorption branch. The pore size distribution of Co(2)CMK-700 shows two peaks centred at 4.1 and 6.8 nm, respectively. As in CMK-5, these two peaks may be assigned to inter-tubular pores (D_{inter}) and inner-tubular pores (D_{inner}), respectively.[9] The D_{inner}-peak intensity decreased progressively as the Co loading increased from Co(2)CMK-700 to Co(5)CMK-700 and Co(10)CMK-700. The progressive decrease of the D_{inner}-peak can be interpreted with the structural change to rod-like frameworks, in good agreement with the above XRD data. Another notable point in the pore size distribution is the appearance of a broad peak around 10–20 nm in Co(10)CMK-700. The average pore

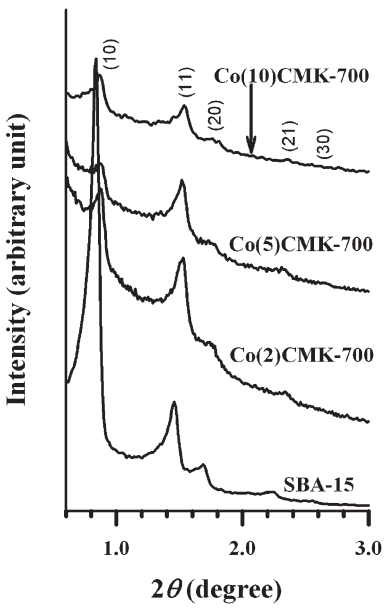

Fig. 1 XRD patterns for mesoporous silica (SBA-15) and mesoporous carbons (CoCMK, synthesized using SBA-15 silica as a template). SBA-15 silica was loaded with $Co(NO_3)_2$ prior to infiltration with the carbon source (furfuryl alcohol). The numbers in parentheses denote Co wt% in template and the numbers at the end denote the carbonization temperatures in °C.

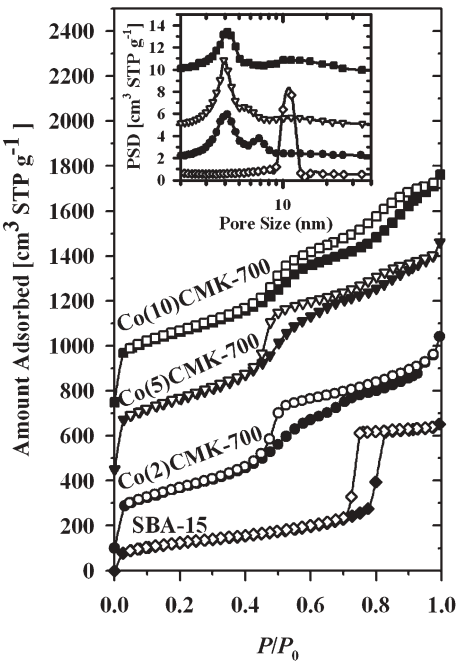

Fig. 2 N_2 adsorption–desorption isotherms for mesoporous silica SBA-15 and CoCMK materials. The isotherms for Co(2)CMK-700, Co(5)CMK-700, and Co(10)CMK-700 are offset vertically by 100, 450, and 750, respectively. The pore diameters, calculated by BJH method from the adsorption branch, are shown in the inset.

Table 1 Structural parameters of SBA-15 silica template and CoCMK mesoporous carbons determined by XRD and N_2 adsorption[a]

	a/nm	S_{BET}/m^2 g^{-1}	D_{inter}/nm	D_{inner}/nm	V_t/cm^3 g^{-1}	$V_{meso} + V_{micro}$/cm^3 g^{-1}
SBA-15	12.3	540	—	11.2	1.18	1.06
Co(2)CMK-700	11.7	1011	4.1	6.9	1.36	0.91
Co(5)CMK-700	11.7	1075	4.1	5.4	1.38	0.83
Co(10)CMK-700	11.7	951	4.2	—	1.24	0.44
Co(2)CMK-900	11.3	1066	4.2	6.8	1.51	1.01
Co(5)CMK-900	11.2	894	4.1	5.4	1.22	0.73
Co(10)CMK-900	11.0	844	4.9	—	1.27	0.38

[a] a, XRD unit cell parameter; S_{BET}, BET specific surface area deduced from the isotherm analysis in the relative pressure range from 0.05 to 0.15; D_{inter}, pore size between adjacent carbon rods or tubes, calculated from the BJH method; D_{inner}, inner pore diameter in the case of tube-like structure, calculated from the BJH method; V_t, total pore volume at a relative pressure of 0.95; $V_{meso} + V_{micro}$, sum of primary mesopore and micropore volumes estimated from α_s plot.

diameter is quite close to the sum of the lattice spacing (a in Table 1) and D_{inter}. Such pores seem to be generated by defects in the OMC frameworks, due to plugging of silica pores by Co nitrate at high loading (0.549 g $Co(NO_3)_2 \cdot 6H_2O$ per g SBA-15, corresponding to 25% of the pore volume).[27] This is further supported by a significant decrease in the total pore volume ($V_{meso} + V_{micro}$) except macropores, with the increase of the Co loading.

Furfuryl alcohol (colourless liquid) changes to a dark brown polymer upon heating to 105 °C in the SBA-15 template containing $Co(NO_3)_2$, which is very similar to the change with heating in a mesoporous aluminosilicate template. The colour change is due to the formation of conjugated double bonds in the polymer.[13] Evidently, the $Co(NO_3)_2$ catalyzes the polymerization of furfuryl alcohol as a Lewis acid inside the template pores. The catalytic polymerization is very important for the OMC synthesis. The framework structure was rod-like in Co(10)CMK-700, but it became relatively more tube-like when the $Co(NO_3)_2$ loading was decreased as in Co(2)CMK-700. The results were very similar for Co(m)CMK-900 samples synthesized at 900 °C. However, without $Co(NO_3)_2$, the synthesis only yielded a product with a featureless XRD pattern.

3.2 Characterization of Co species by XAFS investigation

A series of Co K-edge XANES data were collected after heating Co(5)SBA-15 with furfuryl alcohol. The normalized XANES data are presented in Fig. 3, as a function of heating temperature. The XANES data obtained after polymerization of furfuryl alcohol at 105 °C shows a weak pre-edge absorption peak at 7710 eV (peak A) and the main edge at 7725 eV (peak B). Peak A originates from the transition of 1s electrons to the unoccupied 3d e_g orbital of the Co^{2+} ($T_{2g}^6 e_g^1$) ions.[28] Although the 1s to 3d transition is electric dipole-forbidden in an ideal octahedral symmetry, the appearance of the weak absorption peak can be attributed to electric quadruple coupling and the non-centrosymmetric environment of a distorted Co octahedral site. Peak B is assigned to the electric dipole-allowed transition of a 1s core electron to an unoccupied 4p bound state with T_{1u} symmetry for Co^{2+} ions.[29] The intensity change for peak B may be explained by the replacement of H_2O ligands with conjugate C=C bond systems present in poly(furfuryl alcohol). This is reasonable since the polymerization of furfuryl alcohol is known to acquire conjugated double bonds with loss of H^+ and H^-.[13]

As the temperature was increased to 600 °C, the XANES data showed a gradual decrease in the intensity of peak B. No sign of Co reduction to the metallic state was indicated by the XANES features until 600 °C. However, when the temperature reached 700 °C, the XANES features showed that Co species were completely reduced to Co metal. The Co reduction seemed to be caused by carbon, or reductive gases (such as CO, CH_4, and H_2) generated during the carbonization process.[10]

The Fourier transform (FT) data in Fig. 4 were obtained without a phase shift correction, following the standard analysis procedure using EXAFS data weighted by the wave vector cube (k^3). The FTs for CoO powder and Co foil, which were experimentally obtained in the present work, are also shown as references. The FT data for Co(5)SBA-15 exhibits a peak at 0.20 nm, which can be assigned to the Co–O coordination by H_2O ligands. The EXAFS data for 105 °C indicate no significant changes arising from the presence of furfuryl alcohol polymers in the CoSBA-15 template. The data

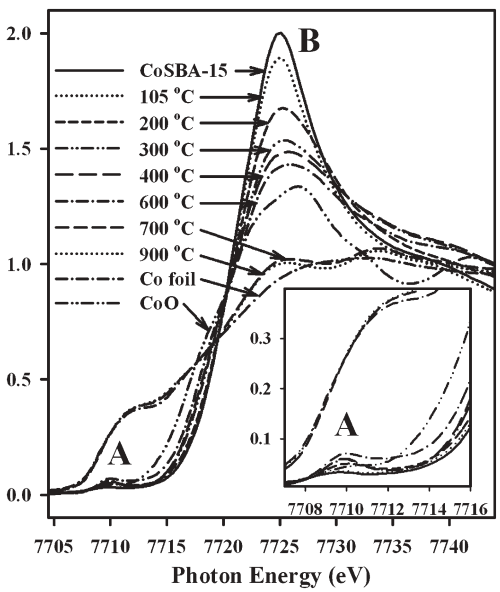

Fig. 3 Normalized Co K-edge XANES taken from SBA-15 silica in various steps for carbon synthesis, where the silica template was loaded with $Co(NO_3)_2$ to give 5 wt% Co loading (CoSBA-15). The CoSBA-15 was infiltrated with furfuryl alcohol and heated to various temperatures. XANES measurements were performed at room temperature. Co foil and CoO were measured for comparison.

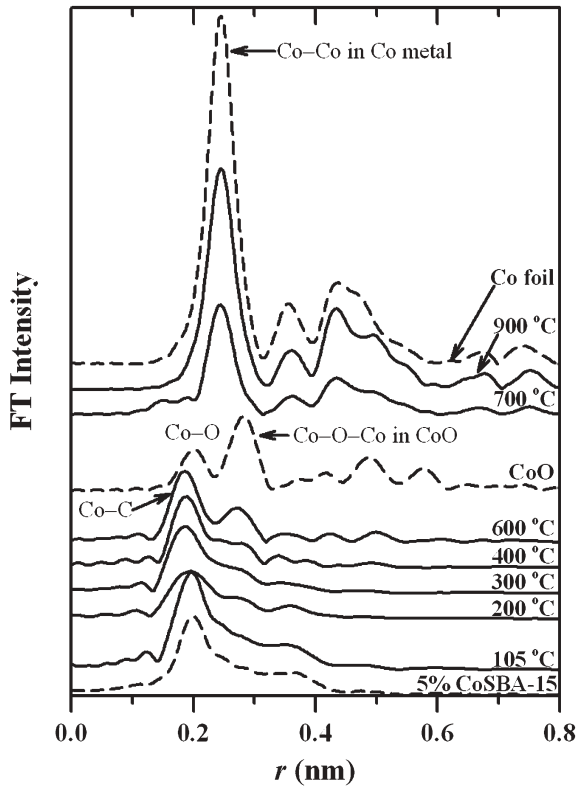

Fig. 4 Fourier transformation of $k^3(k)$-weighted Co K-edge EXAFS without phase shift correction, taken from the mixture of CoSBA-15 and furfuryl alcohol at various stages of carbon synthesis. Sample notations and measurement conditions correspond with those in Fig. 3.

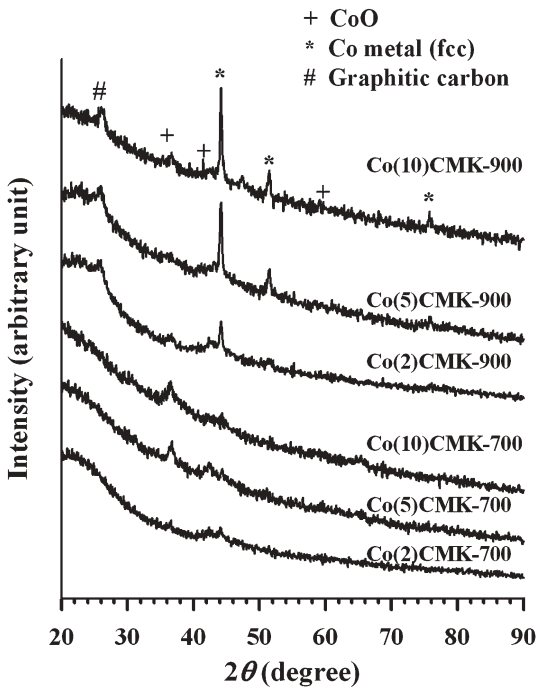

Fig. 5 Wide-angle XRD patterns for CoCMK mesoporous carbons, synthesized using SBA-15 silica as a template.

for the higher temperatures also support the aforementioned interpretation of the XANES data. The broad peak for 200 °C can be assigned to a Co–O peak overlapping a Co–C coordination peak (left shoulder), which is assigned to the Co coordination by the conjugated double-bond system in poly(furfuryl alcohol). The Co–C peak remained until the treatment temperature was increased to 600 °C. However, the Co–C peak disappeared completely after heating at 700 °C. The new peak at 0.24 nm coincided with the Co–Co coordination in Co metal foil, confirming the generation of cobalt nanoparticles at this temperature.

3.3 Co nanoparticles in the OMC structure

As discussed in the previous section, the Co(II) species were completely reduced to cobalt metal at 700 °C during the carbon synthesis. The XRD patterns in Fig. 4 show that the Co metallic phase was partially re-oxidized to Co(II) oxide (CoO), in the Co(*m*)CMK-700 samples. The wide-angle XRD lines in Fig. 5 are assigned to the CoO phase, in addition to the Co metal with the face-centred cubic structure. The CoO phase is attributed to the oxidation of Co particles upon exposure to air at room temperature, and also during the subsequent drying process at 100 °C. The particle size can be estimated from the XRD line broadening, using the Scherrer equation. Despite uncertainties for very fine particles, the information may be valuable for comparative analysis between samples. As the results in Table 2 show, the Co particle size increased with increasing metal loading and carbonization temperature (in the range 14–38 nm). This may be due to sintering of the metal nanoparticles at high loading and temperatures. However, the size of the CoO domain remained almost constant around 5 nm under the same conditions. This result indicates that the Co oxidation by air only occurred at the external 5 -nm layer of the Co nanoparticles.

Fig. 6 shows typical TEM images for Co(*m*)CMK-700 and Co(*m*)CMK-900. The stripe patterns in the background of the images can be assigned to the lattice fringes of the *p6mm* mesostructure of the carbon. The dark spots about 20–100 nm in diameter are the images of the Co–CoO nanoparticles (hereafter 'Co particles' for brevity). It has been confirmed that most of the Co particles were located inside the OMC lattice, from TEM images taken with sample tilting at various angles. The histograms for the particle size distribution and the mean particle sizes in Fig. 5 were determined from 150 samplings of Co particles in each sample, using Digital Micrograph version 3.4.3 distributed by Gatan. The mean particle diameters were 26 ± 6, 25 ± 6, and 23 ± 4 nm for Co(2)CMK-700, Co(5)CMK-700, and Co(10)CMK-700,

Table 2 Co crystal size in CoCMK carbons estimated from XRD line width

	Co metal/nm[a]	CoO/nm[a]
Co(2)CMK-700	14(12)	5(5)
Co(5)CMK-700	22(16)	4(2)
Co(10)CMK-700	24(9)	4(2)
Co(2)CMK-900	23(5)	5(3)
Co(5)CMK-900	28(4)	5(3)
Co(10)CMK-900	38(4)	5(4)

[a] Numbers in parentheses denote standard deviation.

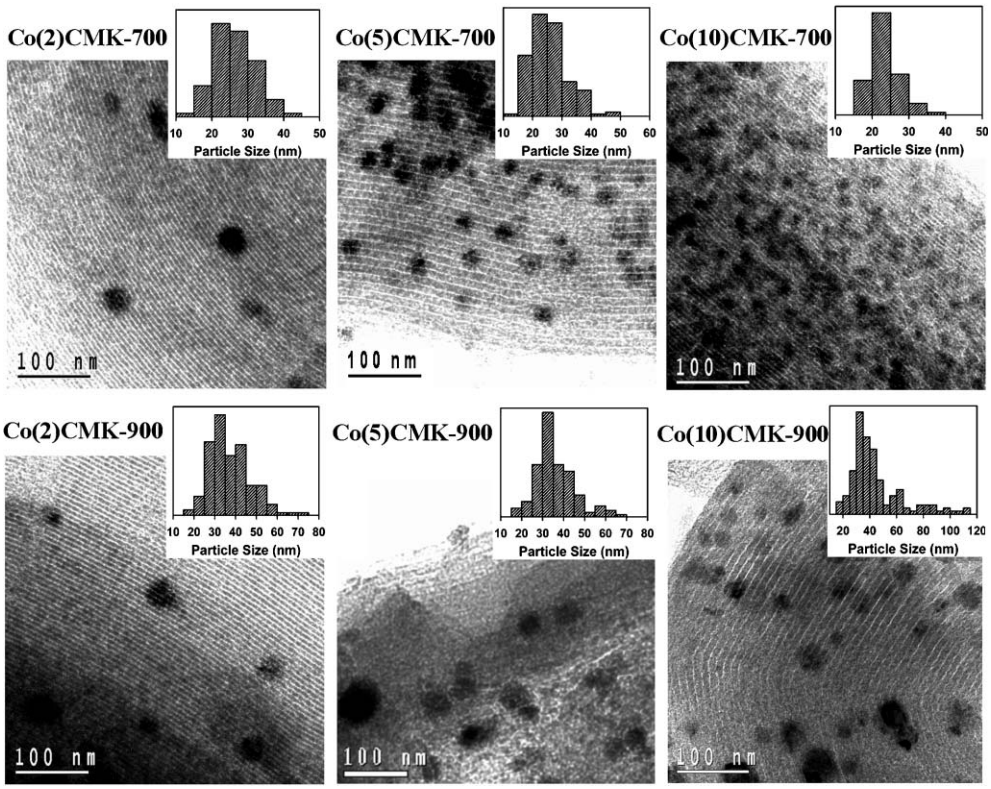

Fig. 6 Typical TEM images of CoCMK materials. Insets show histograms for particle size distributions of partially oxidized Co nanoparticles, which are generated during the carbon synthesis.

respectively. The particle diameters at the corresponding Co loadings increased to 37 ± 10, 36 ± 10, and 56 ± 28 nm, respectively, as the synthesis temperature was increased to 900 °C. These values are very similar the sum of the Co particle size estimated from XRD line broadening and that of the CoO domain. Evidently, the Co particles are much larger than D_{inner}, D_{inter}, or even the lattice parameter (11.0–11.7 nm)of the mesoporous carbons. Such Co particles seemed to grow to these sizes through the interconnecting mesopores.

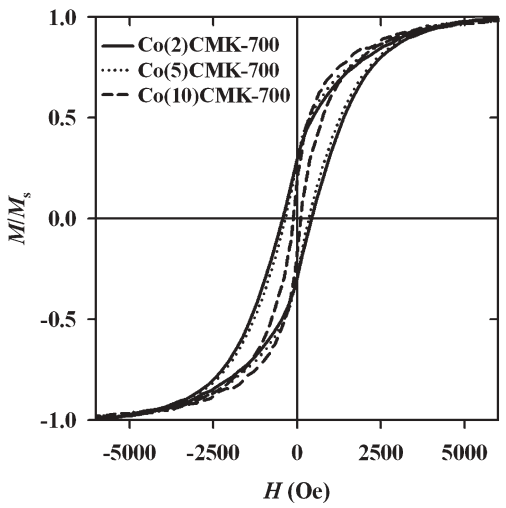

Fig. 7 Normalized magnetization curves for CoCMK materials, measured at 17 °C. M_s values are given in Table 3.

3.4 Magnetic properties and protection against acid leaching

The magnetic properties were characterized by magnetic hysteresis loops with varying magnetic field at 17 °C. As the results in Fig. 7 and Table 3 show, Co particles in the CMK sample exhibited soft ferromagnetic characteristics. The measured coercivity force (H_c) is much smaller than $H_c \sim$ 1000 Oe, which can be estimated for cobalt metal nanoparticles about the same size. This might be due to a CoO layer covering the Co particles, which should be paramagnetic under the present measurement conditions (17 °C) above the Néel temperature of CoO (−3 ± 10 °C).[30] The H_c value might be decreased, due to inclusion of carbon frameworks inside the Co particles. Similarly low H_c characteristics were reported for cobalt nanoparticles encapsulated in carbon.[31,32]

All CoCMK samples synthesized according to the procedures described in section 2.1 exhibited attraction to a Nd–Fe–B hard magnet. The powder samples were separated

Table 3 Magnetic properties of CoCMK carbons obtained from magnetic hysteresis at 17 °C[a]

	M_s/emu g^{-1}	M_r/emu g^{-1}	$S^* = M_r/M_s$	H_c/Oe
Co(2)CMK-700	1.43	0.42	0.30	431
Co(5)CMK-700	1.34	0.39	0.29	350
Co(10)CMK-700	0.34	0.06	0.18	112
Co(2)CMK-900	1.87	0.52	0.28	438
Co(5)CMK-900	5.53	1.38	0.25	420
Co(10)CMK-900	4.98	0.44	0.09	286

[a] M_s, saturation magnetization; M_r, remanence magnetization; S^*, squareness; H_c, coercivity.

from an aqueous slurry upon contacting the magnet onto a vial containing slurry. The sample could be instantaneously re-dispersed by agitation after removal of the magnet. The property of magnetic attraction did not disappear for 1 year after the initial synthesis of CoCMK, under ambient conditions. This property is quite useful for facile separation of mesoporous carbon in catalytic applications and adsorption processes.[15] However, the magnetic separation is known to be suitable only under neutral and basic conditions unless the Co nanoparticles are properly protected. The Co nanoparticles are leached out by strong acids such as HCl and HNO_3. In fact, when we synthesized CoCMK according to the single-step loading of furfuryl alcohol as described in section 2.1, all the samples lost the magnetic attraction completely after washing with 1 M HCl.

Recently, Hyeon *et al.*[16] reported the synthesis of an ordered mesoporous carbon containing Co nanoparticles as a means of magnetic separation, similar to the present study. However, no protection against acid leaching was investigated. Schüth and co-workers[15] supported pre-synthesized Co nanoparticles on ordered mesoporous carbon. They reported that the Co particles could be protected against acid leaching, by coating the Co surface with carbon. Compared with post-synthetic treatment for protection, we have found that self-protected CoCMK samples can be synthesized if furfuryl alcohol is infiltrated in two steps as described in the last paragraph in section 2.1. Acid leaching of the Co(5)CMK-900 sample was measured after slurring in 10 wt% hydrofluoric acid for 4 h and subsequently in an aqueous solution of 1 M HCl for 16 h. Interestingly, the acid-treated sample still maintained sufficient attraction to the Nd–Fe–B magnet for magnetic separation. Elemental analysis after the acid treatment showed 4 wt% Co for 1 g carbon, indicating that nearly 42% of the initial Co was maintained. In addition, the sample showed XRD lines characteristic of the metallic Co phase.

3.5 Carbons with Ni and Fe nanoparticles

NiCMK and FeCMK samples with various metal loadings were also prepared by the same procedure used for CoCMK, except for the changes in nitrate compounds, and their solvents. $Ni(NO_3)_2{\cdot}6H_2O$ was suitable for NiCMK. The Ni compound was dried in vacuum at room temperature and dissolved in acetone. For FeCMK, $Fe(NO_3)_3{\cdot}9H_2O$ was dissolved in ethanol.

The XRD patterns for NiCMK and FeCMK were similar to those for CoCMK (Fig. S2 and S3, ESI†). From the viewpoint of the structural symmetry, the substitution of $Co(NO_3)_2$ with $Ni(NO_3)_2$ or $Fe(NO_3)_3$ did not change the 2-D hexagonal *p6mm* structure of the resultant OMC. However, in the cases of NiCMK and FeCMK, only rod-type carbons were obtained throughout the entire range of the 2–10 wt% metal loading in the silica template, as characterized by the very high (10)/(11) diffraction ratio. This was different from the case of CoCMK, where the carbon structure changed progressively from tube to rod as the metal loading was increased from 2 to 10 wt%. Thus, the results indicate that the detailed carbon framework structures highly depend on the catalyst species and amounts used for the polymerization of furfuryl alcohol.

It seems that the carbon structure (tube- or rod-type) can be controlled by the interaction between the carbon precursor and template pore wall, the template pore diameter, and very importantly, the degree of volume contraction of the carbonizing precursor before it begins to solidify inside the template pores. In the case of CMK-5 synthesis using AlSBA-15 template, the carbonizing poly(furfuryl alcohol) maintains its fluidity until 350 C, at which temperature the carbon precursor has already undergone a significant contraction of volume.[9] The precursor seems to have a high affinity with the template walls. This can lead to the generation of the tube-type carbon.[9] If the Al catalyst is substituted by Co, Ni and Fe, the carbonization behavior of the furfuryl alcohol changes, due to the different acid strength and catalytic activity. A systematic investigation would be necessary for the investigation of the detailed effects. The framework structure can also be affected by various other factors such as the heating scheme for carbonization and reactor pressure following the initial polymerization of furfuryl alcohol. In general, the tube-type carbons were preferentially formed with the enlargement of template pore diameters, and with applying vacuum during the carbonization of poly(furfuryl alcohol).

4. Conclusion

The carbon synthesis using furfuryl alcohol in a mesoporous silica template is a versatile route for obtaining ordered mesoporous carbons with various structures. We have demonstrated that the template-directed method can be extended to the facile synthesis of mesoporous carbons containing transition metal nanoparticles, through the use of SBA-15 silica templates containing $Co(NO_3)_2$, $Ni(NO_3)_2$, and $Fe(NO_3)_3$. Initially, the metal nitrates act as a Lewis acidic catalyst for the polymerization of furfuryl alcohol inside the template pores. The poly(furfuryl alcohol) can then be fully carbonized by heating under a controlled atmosphere at ambient pressure. The carbon framework becomes tube- or rod-like in structure depending on the synthesis conditions. The metal species are spontaneously reduced during the carbonization process, forming metal nanoparticles. The carbon synthesis can be controlled for faithful replication of template structures, where metal nanoparticles are embedded within the carbon structure. In addition, we demonstrated that cobalt nanoparticles are protected against acid dissolution by further addition of furfuryl alcohol prior to complete carbonization. Such ordered mesoporous carbons containing metal nanoparticles may find applications in catalysis and separations requiring magnetic separation.

Acknowledgements

This work was funded by the Creative Research Initiative Programs of the Korean Ministry of Science and Technology, and also through the School of Molecular Science as a part of the Brain Korea 21 Project. Experiments at PLS were supported in part by MOST and POSTECH. The authors are grateful to Prof. Taek Dong Lee at KAIST for measurement of magnetic properties.

References

1 R. Ryoo, S. H. Joo and S. Jun, *J. Phys. Chem. B*, 1999, **103**, 7435.
2 S. Jun, S. H. Joo, R. Ryoo, M. Kruk, M. Jaroniec, Z. Liu, T. Ohsuna and O. Terasaki, *J. Am. Chem. Soc.*, 2000, **122**, 10712.
3 S. H. Joo, S. J. Choi, I. Oh, J. Kwak, Z. Liu, O. Terasaki and R. Ryoo, *Nature*, 2001, **412**, 169.
4 R. Ryoo, S. H. Joo, M. Kruk and M. Jaroniec, *Adv. Mater.*, 2001, **13**, 677.
5 J.-S. Lee, S. H. Joo and R. Ryoo, *J. Am. Chem. Soc.*, 2002, **124**, 1156.
6 W.-H. Zhang, C. Liang, H. Sun, Z. Shen, Y. Guan, P. Ying and C. Li, *Adv. Mater.*, 2002, **14**, 1776.
7 T.-W. Kim, I.-S. Park and R. Ryoo, *Angew. Chem., Int. Ed.*, 2003, **42**, 4375.
8 J. Lee, S. Yoon, T. Hyeon, S. M. Oh and K. B. Kim, *Chem. Commun.*, 1999, 2177.
9 M. Kruk, M. Jaroniec, T.-W. Kim and R. Ryoo, *Chem. Mater.*, 2003, **15**, 2815.
10 E. Fitzer, K. Mueller and W. Schaefer, The Chemistry of the Pyrolytic Conversion of Organic Compounds to Carbon, in *Chemistry and Physics of Carbon*, Marcel Dekker, New York, 1971, vol. 7, pp. 238–376.
11 A. B. Fuertes, *Microporous Mesoporous Mater.*, 2004, **67**, 273.
12 A.-H. Lu, W.-C. Li, W. Schmidt, W. Kiefer and F. Schüth, *Carbon*, 2004, **42**, 2939.
13 M. Choura, N. M. Belgacem and A. Gandini, *Macromolecules*, 1996, **29**, 3839.
14 S. Rahman and H. Yang, *Nano Lett.*, 2003, **3**, 439.
15 A.-H. Lu, W. Schmidt, N. Matoussevitch, H. Böonnemann, B. Spliethoff, B. Tesche, E. Bill, W. Kiefer and F. Schüth, *Angew. Chem., Int. Ed.*, 2004, **43**, 4303.
16 J. Lee, S. Jina, Y. Hwang, J.-G. Park, H. M. Park and T. Hyeon, *Carbon*, 2005, **43**, 2536.
17 S. M. Holmes, P. L. Roberts and J. M. Newton, *Chem. Commun.*, 2005, 1912.
18 A.-H. Lu, W.-C. Li, A. Kiefer, W. Schmidt, E. Bill, G. Fink and F. Schüth, *J. Am. Chem. Soc.*, 2004, **126**, 8616.
19 D. Zhao, J. Feng, Q. Huo, N. Melosh, G. H. Fredrickson, B. F. Chmelka and G. D. Stucky, *Science*, 1998, **279**, 548.
20 M. Choi, W. Heo, F. Kleitz and R. Ryoo, *Chem. Commun.*, 2003, 1340.
21 P. Scherrer, *Nachr. Ges. Wiss. Göttingen, Math.-Phys. Kl.*, 1918, **2**, 96.
22 M. Kruk, M. Jaroniec and K. P. Gadkaree, *J. Colloid Interface Sci.*, 1997, **192**, 250.
23 M. Newville, *J. Synchrotron Radiat.*, 2001, **8**, 322.
24 B. K. Teo, *EXAFS: Basic Principles and Data Analysis*, Springer-Verlag, Berlin, 1986.
25 L. A. Solovyov, T.-W. Kim, F. Kleitz, O. Terasaki and R. Ryoo, *Chem. Mater.*, 2004, **16**, 2274.
26 L. A. Solovyov, A. N. Shmakov, V. I. Zaikovskii, S. H. Joo and R. Ryoo, *Carbon*, 2002, **40**, 2477.
27 A. B. Fuertes and D. M. Nevskaia, *Microporous Mesoporous Mater.*, 2003, **62**, 177.
28 H. C. Choi, S. Y. Lee, S. B. Kim, M. G. Kim, M. K. Lee, H. J. Shin and J. S. Lee, *J. Phys. Chem. B*, 2002, **106**, 9252.
29 W. S. Yoon, K. B. Kim, M. G. Kim, M. K. Lee, H. J. Shin, J. M. Lee, J. S. Lee and C. H. Yo, *J. Phys. Chem. B*, 2002, **106**, 2526.
30 T. F. Connolly and E. D. Copenhaver, *Bibliography of Magnetic Materials and Tabulation of Magnetic Transition Temperatures*, Plenum, New York, 1972, vol. 5, p. 34.
31 S. Gangopadhyay, G. C. Hadjipanayis, C. M. Sorensen and K. J. Klabunde, *IEEE Trans. Magn.*, 1992, **28**, 3174.
32 J.-M. Bonard, S. Seraphin, J.-E. Wegrowe, J. Jiao and A. Châtelain, *Chem. Phys. Lett.*, 2001, **343**, 251.